OPTICA

Full-bandwidth quantum memory of squeezed light

Jinxian Guo,[1,2,†] Meihong Wang,[3,4,†] Zeliang Wu,[5] Chenyu Qiao,[3,4] Fengyi Xu,[3,4] Xiaoran Zhang,[3,4] Xiaolong Su,[3,4,8] Liqing Chen,[5,6,9] and Weiping Zhang[1,2,4,6,7,10]

[1]School of Physics and Astronomy, Shanghai Jiao Tong University, Shanghai 200240, China
[2]Tsung-Dao Lee Institute, Shanghai Jiao Tong University, Shanghai 200240, China
[3]State Key Laboratory of Quantum Optics Technologies and Devices, Institute of Opto-Electronics, Shanxi University, Taiyuan 030006, China
[4]Collaborative Innovation Center of Extreme Optics, Shanxi University, Taiyuan 030006, China
[5]School of Physics, East China Normal University, Shanghai 200062, China
[6]Shanghai Branch, Hefei National Laboratory, Shanghai 201315, China
[7]Shanghai Research Center for Quantum Sciences, Shanghai 201315, China
[8]suxl@sxu.edu.cn
[9]lqchen@phy.ecnu.edu.cn
[10]wpz@sjtu.edu.cn
[†]These authors contributed equally to this work.

Received 15 September 2025; revised 7 April 2026; accepted 8 April 2026; published 29 April 2026

Achieving high end-to-end efficiency and broadband quantum memory of squeezed light is crucial for continuous-variable quantum information processing. Existing demonstrations fail to store squeezed states across their full squeezing bandwidth. Here, we present a full-bandwidth quantum memory of squeezed light with up to 24 MHz bandwidth, which is at least 12 times that of previous narrowband resonant memory systems, via a far-off resonant Raman process. We achieve output squeezing as high as 1.0 ± 0.29 dB, with fidelity above 92 ± 0.5% and a memory efficiency of 80%, corresponding to an end-to-end efficiency of 64.2 ± 0.7% when input squeezing is 1.6 ± 0.23 dB. The lowest excess noise of 0.025 shot-noise unit in the memory system is estimated by the noisy model, which benefits from optimizing quantum memory performance with a backward-retrieval strategy. Our results show high-performance memory for squeezed states within tens of MHz-level bandwidth, which has potential applications in high-speed quantum information processing. © 2026 Optica Publishing Group under the terms of the Optica Open Access Publishing Agreement

https://doi.org/10.1364/OPTICA.578380

1. INTRODUCTION

In quantum information science, synchronizing and buffering information in space or time makes quantum memory a key component for long-distance quantum communication networks and scalable quantum computation [1–3]. Bandwidth, end-to-end efficiency (including the transmission efficiency of the optical path), and fidelity of quantum memory jointly determine the attainable communication distance, the tolerable loss, and the depth of computation. Considering that contemporary quantum processors and high-speed networks already run at clock rates of MHz–GHz, the quantum memory whose bandwidth is below this scale truncates high-frequency sidebands and directly reduces channel capacity [4]. Improvements in both efficiency and fidelity of quantum memory exponentially enlarge the loss of photons that the network can withstand [5,6]. Even a percent-level loss in end-to-end efficiency can suppress the quantum bit rate by orders of magnitude and halve the communication distance in a nested quantum-repeater architecture [7,8].

To date, significant advances in the storage of discrete-variable qubits or weak coherent states have been achieved [9–15]. Beyond these, continuous-variable (CV) states, particularly squeezed light, offer efficient state manipulation [1], making them critical for high-speed quantum communication and scalable quantum computation [1,16]. However, current squeezed-light memories are limited to MHz-level bandwidth in narrowband systems (e.g., electromagnetically induced transparency (EIT) [17–20] or quantum non-demolition measurement of spins [21]. The inherent narrow bandwidth of these systems hinders the storage of squeezed light across its full bandwidth, leading to the loss of high-frequency information of quantum states and lower computational fidelity. Moreover, the low end-to-end efficiency and fidelity of the quantum memory for squeezed light leave the quantum advantage of squeezed states inaccessible. Consequently, achieving high end-to-end efficiency, low noise, and genuinely full-bandwidth storage of broadband squeezed light remains the decisive test for universal quantum memory.

Far-off resonance Raman quantum memory offers a promising platform for broadband quantum state storage by circumventing the bandwidth limitations of resonant approaches. Up to now, significant progress has been made in storing weak coherent pulses and single photons, including GHz-bandwidth storage [13,22], efficiency improvements via optimization techniques [9], and noise suppression advancements [11,23–27]. However, these developments have not yet met the requirements for squeezed-state storage, which demands strict concurrent performance of

high end-to-end efficiency and near-zero excess noise to preserve quantum properties across a broad bandwidth. To date, high-efficiency quantum memory for broadband squeezed light remains unrealized.

In this work, we demonstrate the full-bandwidth write-in and retrieval of a squeezed vacuum state using a Raman memory in an atomic vapor. We develop a backward-retrieval strategy and a dual-pulse time-domain homodyne tomography technique to solve the technical challenges of quantum state characterization and quantum memory performance optimization, respectively. The memory efficiency of 80% and the excess noise of 0.025 shot-noise unit (SNU) are achieved by a backward-retrieval strategy, which is estimated by a noisy channel model. For an input squeezed light pulse with a noise reduction of 1.6 ± 0.23 dB, the retrieved state maintains a noise reduction of 1.0 ± 0.29 dB, achieving the highest level of squeezing for a retrieved pulse. Furthermore, we also demonstrate the full-bandwidth quantum memory of squeezed state with a maximum bandwidth of 24 MHz. Benefiting from the high-efficiency and low-noise memory system, the fidelity of the retrieved signal exceeds 92% even when operating at a bandwidth more than an order of magnitude larger than previously reported systems [17–20]. These results represent a significant advancement toward the realization of high-performance CV quantum technologies, including quantum computing, squeezing-enhanced quantum metrology, and quantum communication.

2. EXPERIMENTAL SETUP

As shown in Fig. 1(a), the experimental setup of full-bandwidth squeezed light quantum memory consists of three parts, which are the squeezer, the memorizer, and the homodyne detection system, respectively. In the part of the squeezer, an optical parametric amplifier (OPA) is used to generate the squeezed vacuum state. A 795 nm laser with the blue-detuned 1.6 GHz frequency from the ^{87}Rb atomic transition $|5S_{1/2}, F=2\rangle \rightarrow |5P_{1/2}, F'=2\rangle$, passes through an acousto-optic modulator (AOM1) to produce the pulsed light with a full-width-at-half-maximum (FWHM) of 227.2 ns. The pulsed light is seeded into a second-harmonic generator (SHG) to generate a pulsed beam at 397.5 nm, which serves as the pump beam of the OPA. The detailed parameters of SHG and OPA can be found in Section 1 of Supplement 1. Under the de-amplification condition of OPA [28] with a pump power of 25 mW, an amplitude-squeezed state is generated with a squeezing bandwidth of 15 MHz. As shown in Fig. 1(b), the noise of amplitude quadrature ($\hat{x} = (\hat{a} + \hat{a}^\dagger)/\sqrt{2}$) and phase quadrature ($\hat{p} = (\hat{a} - \hat{a}^\dagger)/\sqrt{2}i$) of the squeezed state are squeezed and anti-squeezed, respectively, where $\hat{a}^\dagger$ and $\hat{a}$ are the creation and annihilation operators.

In the part of the memorizer, a ^{87}Rb atomic ensemble is initially prepared in the state $|5S_{1/2}, F=2\rangle$ by a 780 nm pumping laser with FWHM of 45 μs. The squeezed vacuum state $\hat{a}_{\text{in}}$ is co-injected with a write pulse into the atomic ensemble to perform the Raman write process, when the flip mirror (FM) is flipped down. The write pulse shaped by the AOM2 is two-photon resonant with $\hat{a}_{\text{in}}$ in the atomic ensemble, as illustrated in the inset of Fig. 1(a). After the write process, a read pulse with FWHM of 105 ns, shaped by AOM4 with the red-detuned frequency of 2 GHz from the atomic transition $|5S_{1/2}, F=1\rangle \rightarrow |5P_{1/2}, F'=1\rangle$, is injected into the atomic ensemble to retrieve the squeezed vacuum state $\hat{a}_{\text{out}}$. Figure 1(c) shows the temporal waveforms of the input state, write, read, and output state of the memory process. The bandwidth of the output state reaches 43.1 MHz (corresponding to a FWHM of 23 ns), which is high enough for the full-bandwidth memory of the squeezed state.

In the experiment, we solve two technical challenges, which are achieving a high-efficiency, low-noise Raman quantum memory and characterization of the quantum properties of the squeezed states, respectively, to achieve the full-bandwidth quantum

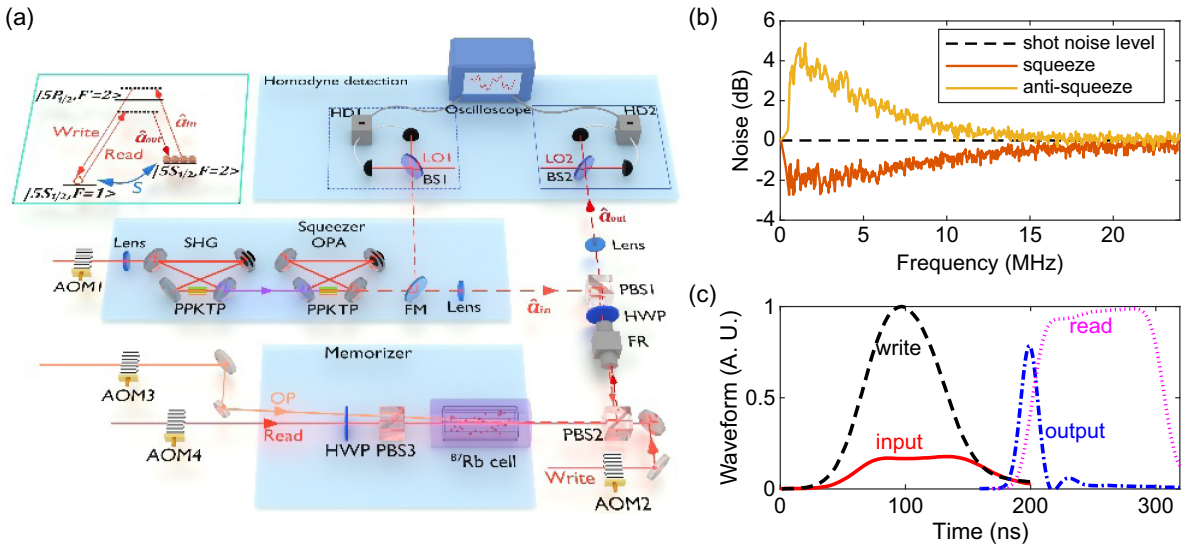

Fig. 1. (a) Experimental setup of quantum memory. AOM, acousto-optical modulator; SHG, second-harmonic generator; OPA, optical parametric amplifier; PPKTP, periodically poled $KTiOPO_4$; FM, flip mirror; OP, optical pumping; FR, Faraday rotator; HWP, half-wave plate; PBS, polarized beam splitter; BS, beam splitter; LO, local oscillator; and HD, homodyne detector. The inset at left corner shows the atomic-level configuration. The atomic vapor is 7.5 cm long and heated to 89°C, resulting in an optical depth of approximately 1200. The power of the write and read lights are 240 and 13 mW, respectively. The signal, write, and read beams have beam diameters of 0.5, 1.1, and 1.1 mm, respectively. (b) The relative noise power spectrum of a CW squeezed vacuum state. The squeezing sidebands expand to 15 MHz. (c) Temporal waveforms of the input squeezed vacuum state ($\hat{a}_{\text{in}}$), the retrieved squeezed vacuum pulse ($\hat{a}_{\text{out}}$), the write pulse, and the read pulse in the experiment.

memory of the squeezed state. To solve the first technical challenge, we apply a backward-retrieval Raman memory strategy. In the write process, the waveform of the write pulse should be adjusted to achieve a precise temporal mode matching between the input signal and the write pulse, which improves the write-in efficiency [9]. Specifically, we use a strong coherent probe with the same temporal envelope as the squeezed vacuum and iteratively update the temporal waveform of the write pulse using a differential evolution (DE) algorithm to maximize the write-in efficiency [29]. In the read process, we use a backward-propagating read light [as shown in Fig. 1(a)] to extract the signal from the atomic ensemble. Compared to the conventional forward retrieval strategy [9], backward-retrieval implements the time-reversed process of the write process and is therefore optimal [30], ensuring a high efficiency with significantly low read power (the details are provided in Section 2 of Supplement 1). In contrast, four-wave mixing (FWM) noise arises from atom–light FWM coupling, whose coupling strength scales with the read power. By operating at a substantially low read power, backward retrieval reduces the coupling strength of FWM and consequently suppresses FWM noise. Thus, the loss and four-wave mixing (FWM) noise amplification are reduced by the backward-retrieval strategy.

To solve the second challenge of characterizing the quantum properties of squeezed states, we develop a dual-pulse time-domain homodyne tomography technique to obtain the temporal waveform and phase of a weak signal, which is difficult in conventional time-domain homodyne tomography [18] due to the low photon number of the measured quantum state (<0.1 photons/pulse). In our method, we use two temporally separated memory cycles within the same experimental run: (i) a squeezed vacuum pulse (first cycle) for quantum state measurement, and (ii) a bright coherent pulse (second cycle) with identical temporal shape but delayed by τ (here we choose $\tau = 500$ ns) to track the optical phase via interference fringes. Since phase drifts typically occur at a low frequency ($\leq$100 kHz), the effect of delay τ on phase estimation can be ignored.

To reconstruct the input state $\hat{a}_{\text{in}}$, the input squeezed vacuum pulse in the first cycle interferes with the local oscillator (LO1) on HD1 to acquire the homodyne photocurrent. The temporal waveform of the input state is obtained through a point-wise calculation of the variance of the homodyne photocurrent. Then the quadrature value is obtained by integrating the production of the photocurrent and the temporal waveform [18]. The phase of the squeezed vacuum state is determined by acquiring the interference fringe of the coherent pulse in the second cycle on HD1.

To reconstruct the output state $\hat{a}_{\text{out}}$, the squeezed vacuum pulse is stored and retrieved in the atomic ensemble in the first cycle, followed by storage and retrieval of the delayed coherent reference pulse in the second cycle. The retrieved squeezed state and coherent reference are sequentially sent to HD2 to obtain the homodyne photocurrent and interference phase, respectively. Since the phase of the retrieved state is tracked according to the phase of the retrieved coherent light, the systematic Stark shifts introduced by quantum memory can be canceled.

3. MEMORY PERFORMANCE

We evaluate the performance of quantum memory by analyzing the quadratures and Wigner functions of the input and output states, as shown in Fig. 2. The measured quadrature values of the input and output states are shown in Fig. 2(a) when the FWHM of

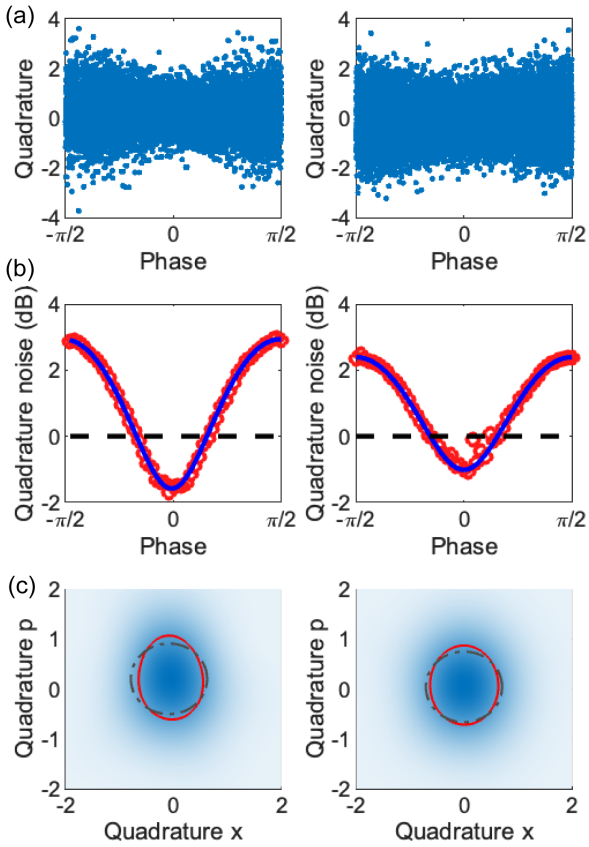

Fig. 2. (a) Experimental data of phase-dependent quadrature values. Left and right columns represent the input and retrieved states, respectively. (b) Results of quadrature variances. The red circles represent the variances obtained from experimental quadrature values, and the solid lines are the corresponding fittings. (c) Contour plots of Wigner functions. The black circles represent the vacuum state, and the red circles are the squeezed vacuum states. The small offset originates from a minor leakage of coherent light during the squeezed vacuum state generation, which does not affect the squeezing level.

the input state is 227.5 ns. The noise fluctuations of the amplitude quadrature (phase 0) of the states $\hat{a}_{\text{in}}$ and $\hat{a}_{\text{out}}$ are narrower than those of the shot-noise level and the amplitude quadrature (phase $\pi/2$), which means that the input and output states of the quantum memory are both squeezed states. Based on the quadrature data, we obtain the quadrature variances of the input and output states, respectively, as shown in Fig. 2(b). The input state's minimum quadrature noise is 1.6 ± 0.23 dB lower than the shot-noise level (SNL, black-dashed line), whereas the output state remains 1.0 ± 0.29 dB below the SNL. In the current system, the end-to-end efficiency is $64.2 \pm 0.7\%$, including the memory efficiency of 80% and the optical transmission efficiency of 80.3%. Using the quadrature data, we reconstruct the Wigner functions of the input and output states via the maximum likelihood estimation for quantum state tomography (detailed in Section 3 of Supplement 1) [31], as shown in Fig. 2(c).

Based on the Wigner functions, we obtain the unconditional fidelity $F = \text{Tr}[(\rho_{\text{in}}^{1/2}\rho_{\text{out}}\rho_{\text{in}}^{1/2})^{1/2}]^2$ of the memory system by calculating the overlap between the input density matrix ρ_{in} and the output states ρ_{out}, which reaches 97.9% confirming that our memory effectively preserves the quantum properties of the input state. For a fair assessment, we calculated the fidelity between the input squeezed state (1.6 dB) and the vacuum state by

$F = \mathrm{Tr}[(\rho_{\mathrm{in}}^{1/2}\rho_{\mathrm{vac}}\rho_{\mathrm{in}}^{1/2})^{1/2}]^2 = 83.4\%$, which is significantly lower than the measured input–output fidelity of 97.9% in our Raman memory process.

Since the performance of quantum memory is also influenced by the noise level in the memory process, it is important to characterize the excess noise of the memory system. When the squeezed vacuum state passes through the memory system, the output state can be described by (detailed in Section 4 of Supplement 1)

$$\hat{a}_{\mathrm{out}} = \sqrt{\eta}\hat{a}_{\mathrm{in}} + \sqrt{1-\eta}\hat{v} + \hat{b}_{\mathrm{th}}, \tag{1}$$

where η is the end-to-end efficiency of the memory, $\hat{b}_{\mathrm{th}}$ and $\hat{v}$ are the operators of the thermal and vacuum states, respectively. The excess noise δ is introduced independently since it acts as a nondegenerate amplification, which is mainly due to the FWM process in Raman memory. Based on the measured variances of the input and output quadratures, we estimate the excess noise in the memory process by the variance of the thermal state $\hat{b}_{\mathrm{th}}$ according to Eq. (1), which is as low as $\delta = 0.025$ SNU under the condition that the FWHM of the input state is 227.5 ns.

An important advantage of Raman memory is that it enables one to store the signal with a GHz-level bandwidth. To showcase its broadband capability, we store squeezed states with different bandwidths, which are prepared by reducing the pump pulse duration for SHG. In this case, the squeezed vacuum states $\hat{a}_{\mathrm{in}}$ with FWHM varying from 227.2 to 41.6 ns (corresponding to a bandwidth of 4.4–24 MHz) are prepared, whose squeezing level varies from 1.6 to 0.9 dB, as shown in Fig. 3(a). After quantum memory, the retrieved states consistently exhibit noise levels below the SNL, which covers the full bandwidth of the squeezed vacuum state. At 24 MHz bandwidth, the output state retains 0.55 ± 0.22 dB of squeezing despite the input signal's 0.9 ± 0.3 dB squeezing, corresponding to a memory fidelity of 97.6%. The 24 MHz bandwidth is 12 times larger than the previous EIT-based system. To better demonstrate the broadband capability of the memory system, we further test the unconditional fidelity change with input signal bandwidth, as shown in Fig. 3(b). The unconditional fidelity exceeds 92% in the bandwidth range from 4.4 to 24 MHz.

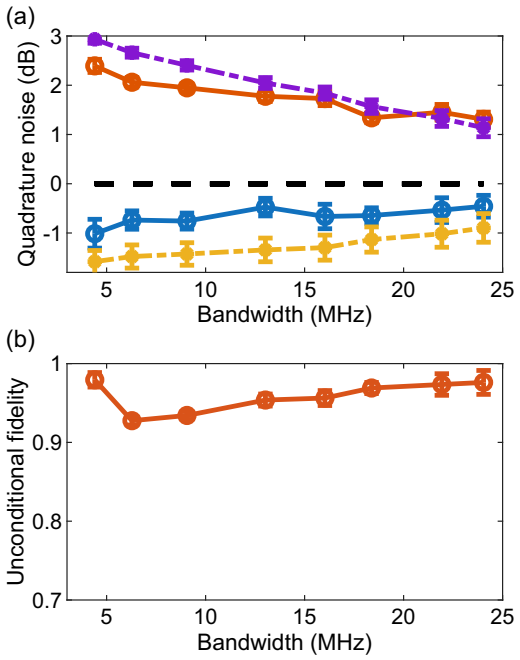

Fig. 3. (a) The dependence of the squeezing level of input and retrieved states on the bandwidth of the input state. The yellow (blue) and purple (red) datapoints represent the squeezing and anti-squeezing of input (retrieved) states. (b) The dependence of unconditional fidelity of the memory process on the bandwidth of the input state.

Furthermore, we evaluate end-to-end efficiency η and excess noise δ for input states with different bandwidths, as shown in Table 1. Since the memory parameters (e.g., control pulse power and temporal mode matching between signal and control) are optimized globally across bandwidths, small systematic variations in efficiency, and excess noise can occur. Importantly, the end-to-end efficiencies do not decrease significantly with the increase of bandwidth, and excess noises are typically around 0.027 SNU, ensuring a high squeezing level of the retrieved state. These results demonstrate that current memory is capable of storing the squeezed state across the full squeezing bandwidth.

4. CONCLUSION

In summary, we experimentally demonstrate a high-performance memory of the squeezed vacuum states across the full squeezing bandwidth with Raman quantum memory. By applying a backward retrieval strategy, we realize a Raman quantum memory with a memory efficiency of 80% and excess noise of 0.025 SNU, which provides a high-efficiency and low-noise quantum memory of the squeezed state. Utilizing a dual-pulse time-domain homodyne tomography, we obtain the retrieval state with a maximum squeezing of 1.0 ± 0.29 dB when a squeezed state with only 1.6 ± 0.23 dB squeezing is applied as the input state. To further highlight the broadband capability of current Raman memory, we expand the bandwidth of input states to 24 MHz and achieve 0.55 ± 0.22 dB output squeezing when the input squeezing is 0.9 ± 0.3 dB. All unconditional fidelities for squeezed states with different bandwidths exceed 92%, which exceeds the previously reported result in squeezed state memory demonstration [18], confirming the successful memory of squeezed states across their full bandwidth.

The high efficiency of Raman memory protects the state from loss, and its low-noise property protects the state from the contamination of excess noise. Importantly, both the end-to-end efficiency and excess noise remain stable across the 4–24 MHz bandwidth range, demonstrating that the memory performance is bandwidth-independent and can be extended to even larger bandwidths without significant noise degradation. The performance of the memory system can be further optimized by reducing end-to-end losses and

Table 1. Parameters of Bandwidth *B* (MHz), the End-to-End Efficiency η, and the Excess Noise δ (SNU) in the Memory Process

B	4.4	6.28	9.06	13.0	16.0	18.4	21.9	24.0
η	0.642 ± 0.007	0.635 ± 0.011	0.666 ± 0.009	0.630 ± 0.016	0.742 ± 0.024	0.629 ± 0.026	0.663 ± 0.032	0.757 ± 0.045
δ	0.025 ± 0.029	0.026 ± 0.008	0.023 ± 0.013	0.047 ± 0.027	0.038 ± 0.030	0.013 ± 0.023	0.025 ± 0.029	0.021 ± 0.024

excess noise. Furthermore, the storage time can be improved in the future. In our experiment, the storage time is 250 ns (detailed in Supplement 1), which can be further improved by enlarging the beam diameter and using a mm-level-diameter paraffin-coated atomic cell to the hundreds-of-microseconds level [32]. In practice, the increasing beam size could lead to reduced Rabi frequencies of the write and read fields, which may in turn affect the memory bandwidth and efficiency. Appropriate adjustments of the control power or other memory parameters can mitigate these effects. We note that increasing the beam size could reduce the Rabi frequencies of the write and read fields, which may in turn affect the memory bandwidth and efficiency; this effect can be mitigated, for example, by adjusting the control power or other memory parameters. Additionally, the broadband nature of Raman memory enables a higher bandwidth of the retrieved state than that of the input signal, since the bandwidth of the retrieved state is determined by the read pulse [9]. In this experiment, a 4.4 MHz squeezed vacuum state input yields a 43.1 MHz squeezed vacuum state output, representing a significant bandwidth enhancement. This provides a novel approach for high-performance quantum state conversion interfaces, which has potential applications in time-multiplexing CV quantum information processing.

Funding. Quantum Science and Technology-National Science and Technology Major Project (2021ZD0303201); National Natural Science Foundation of China (12434015, 12374331, 12274132, 62275145, U23A2075, 12234014, 11654005); Shanghai Municipal Science and Technology Major Project (2019SHZDZX01); Innovation Program of Shanghai Municipal Education Commission (202101070008E00099); National Key Research and Development Program of China (2016YFA0302001); Shanghai Talent Program; Fund for Shanxi "1331 Project" Key Subjects Construction.

Acknowledgment. W.Z. acknowledges additional support from the Shanghai Talent Program.

Disclosures. The authors declare no conflicts of interest.

Data availability. Data underlying the results presented in this paper are not publicly available at this time but may be obtained from the authors upon reasonable request.

Supplemental document. See Supplement 1 for supporting content.

REFERENCES

1. S. L. Braunstein and P. van Loock, "Quantum information with continuous variables," Rev. Mod. Phys. **77**, 513–577 (2005).
2. C. Weedbrook, S. Pirandola, R. García-Patrón, *et al.*, "Gaussian quantum information," Rev. Mod. Phys. **84**, 621–669 (2012).
3. X.-B. Wang, T. Hiroshima, A. Tomita, *et al.*, "Quantum information with Gaussian states," Phys. Rep. **448**, 1–111 (2007).
4. Y. Shiozawa, J.-I. Yoshikawa, S. Yokoyama, *et al.*, "Quantum nondemolition gate operations and measurements in real time on fluctuating signals," Phys. Rev. A **98**, 052311 (2018).
5. S. Pirandola, R. Laurenza, C. Ottaviani, *et al.*, "Fundamental limits of repeaterless quantum communications," Nat. Commun. **8**, 15043 (2017).
6. S. Pirandola, U. L. Andersen, L. Banchi, *et al.*, "Advances in quantum cryptography," Adv. Opt. Photonics **12**, 1012–1236 (2020).
7. N. Sangouard, C. Simon, H. de Riedmatten, *et al.*, "Quantum repeaters based on atomic ensembles and linear optics," Rev. Mod. Phys. **83**, 33–80 (2011).
8. S. Muralidharan, L. Li, J. Kim, *et al.*, "Optimal architectures for long distance quantum communication," Sci. Rep. **6**, 20463 (2016).
9. J. Guo, X. Feng, P. Yang, *et al.*, "High-performance Raman quantum memory with optimal control in room temperature atoms," Nat. Commun. **10**, 148 (2019).
10. O. Davidson, O. Yogev, E. Poem, *et al.*, "Single-photon synchronization with a room-temperature atomic quantum memory," Phys. Rev. Lett. **131**, 033601 (2023).
11. D. G. England, K. A. Fisher, J.-P. W. MacLean, *et al.*, "Storage and retrieval of THz-bandwidth single photons using a room-temperature diamond quantum memory," Phys. Rev. Lett. **114**, 053602 (2015).
12. P. S. Michelberger, T. F. M. Champion, M. R. Sprague, *et al.*, "Interfacing GHz-bandwidth heralded single photons with a warm vapour Raman memory," New J. Phys. **17**, 043006 (2015).
13. K. A. G. Fisher, D. G. England, J.-P. W. MacLean, *et al.*, "Frequency and bandwidth conversion of single photons in a room-temperature diamond quantum memory," Nat. Commun. **7**, 11200 (2016).
14. D.-S. Ding, W. Zhang, Z.-Y. Zhou, *et al.*, "Quantum storage of orbital angular momentum entanglement in an atomic ensemble," Phys. Rev. Lett. **114**, 050502 (2015).
15. D.-S. Ding, W. Zhang, Z.-Y. Zhou, *et al.*, "Raman quantum memory of photonic polarized entanglement," Nat. Photonics **9**, 332–338 (2015).
16. U. L. Andersen, T. Gehring, C. Marquardt, *et al.*, "30 years of squeezed light generation," Phys. Scripta **91**, 053001 (2016).
17. K. Honda, D. Akamatsu, M. Arikawa, *et al.*, "Storage and retrieval of a squeezed vacuum," Phys. Rev. Lett. **100**, 093601 (2008).
18. J. Appel, E. Figueroa, D. Korystov, *et al.*, "Quantum memory for squeezed light," Phys. Rev. Lett. **100**, 093602 (2008).
19. Z. Yan, L. Wu, X. Jia, *et al.*, "Establishing and storing of deterministic quantum entanglement among three distant atomic ensembles," Nat. Commun. **8**, 718 (2017).
20. M. Arikawa, K. Honda, D. Akamatsu, *et al.*, "Quantum memory of a squeezed vacuum for arbitrary frequency sidebands," Phys. Rev. A **81**, 021605 (2010).
21. K. Jensen, W. Wasilewski, H. Krauter, *et al.*, "Quantum memory for entangled continuous-variable states," Nat. Phys. **7**, 13–16 (2011).
22. K. F. Reim, J. Nunn, V. O. Lorenz, *et al.*, "Towards high-speed optical quantum memories," Nat. Photonics **4**, 218–221 (2010).
23. D. J. Saunders, J. H. D. Munns, T. F. M. Champion, *et al.*, "Cavity-enhanced room-temperature broadband Raman memory," Phys. Rev. Lett. **116**, 090501 (2016).
24. K. Zhang, J. Guo, L. Chen, *et al.*, "Suppression of the four-wave-mixing background noise in a quantum memory retrieval process by channel blocking," Phys. Rev. A **90**, 033823 (2014).
25. S. E. Thomas, T. M. Hird, J. H. Munns, *et al.*, "Raman quantum memory with built-in suppression of four-wave-mixing noise," Phys. Rev. A **100**, 033801 (2019).
26. M. D. browski, R. Chrapkiewicz, and W. Wasilewski, "Hamiltonian design in readout from room-temperature Raman atomic memory," Opt. Express **22**, 26076–26091 (2014).
27. Z. Yu, Z. Wu, X. Li, *et al.*, "Interferometry-integrated noise-immune quantum memory," Phys. Rev. Lett. **131**, 150804 (2023).
28. M. Wang, M. Zhang, Z. Qin, *et al.*, "Experimental preparation and manipulation of squeezed cat states via an all-optical in-line squeezer," Laser Photonics Rev. **16**, 2200336 (2022).
29. S. Ming, J. Guo, Y. Wu, *et al.*, "Optimizing Raman quantum memory with dynamic phase," Sci. China Inf. Sci. **66**, 180505 (2023).
30. J. Guo, Z. Wu, G. Bao, *et al.*, "Near-perfect broadband quantum memory enabled by intelligent spin-wave compaction," Phys. Rev. Lett. **135**, 170802 (2025).
31. A. I. Lvovsky, "Iterative maximum-likelihood reconstruction in quantum homodyne tomography," J. Opt. B **6**, S556–S559 (2004).
32. Z. Wu, J. Guo, Z. Yu, *et al.*, "AI-assisted hyper-dimensional broadband quantum memory with efficiency above 90% in warm atoms," npj Quantum Inf. **11**, 136 (2025).